Industrial Crops & Products 187 (2022) 115544

Contents lists available at ScienceDirect

Industrial Crops & Products

journal homepage: www.elsevier.com/locate/indcrop

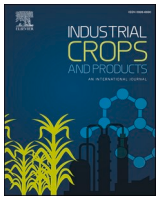

Hydrogen production by organic waste chemical looping gasification (OW-CLG) enhanced by V2O3 catalysed reforming via partial oxidation approach

Zongming Zheng [a], Laixing Luo [a], Xing Zheng [a], Ruonan Duan [a], Xianbin Xiao [a], Changqing Dong [a,b], Wu Qin [a,*]

[a] National Engineering Research Center of New Energy Power Generation, School of New Energy, North China Electric Power University, Beijing 102206, China
[b] State Key Laboratory of Alternate Electrical Power System with Renewable Energy Sources, North China Electric Power University, Beijing 102206, China

ARTICLE INFO

Keywords:
Biomass
Chemical looping gasification
Hydrogen
Liquid waste

ABSTRACT

Biomass and distillery wastewater are promising sources to produce H_2-rich syngas through the thermal conversion. We propose the organic waste chemical looping gasification (OW-CLG) scheme for hydrogen production with straw stalk and concentrated distillery wastewater as feedstock. V_2O_3 was employed to promote methane reforming and enhance the efficiency of hydrogen production by partially oxidation. Experiments under different temperatures (T) and the molar ratio of V_2O_3 to CH_4 ($n_{V_2O_3}/n_{CH_4}$) are performed in details. The results show that the above parameters have a significant effect on OW-CLG process. The optimal methane conversion rate of 44.9 % is obtained at oxygen excess ratio, temperature, and $m_{V_2O_3}/m_{corn\ stalk}$ of 0.2, 700 ℃, and 2.16 respectively. The highest H_2 yield is 2.05 l with 1 g corn stalk and 20 ml ethanol model solution. The reaction kinetics and the thermodynamics were analyzed, verifying that the introduction of ethanol liquid waste and V_2O_3 could boost hydrogen generation. The corn stalk OW-CLG is an endothermic process with the total endothermic heat of 5.396 kJ/mol. The thermodynamically feasible temperature range for the partial oxidation of CH_4 to hydrogen by V_2O_3 is above 950 K. V_2O_3 OC during OW-CLG is regenerated by the reaction of VC and CO_2.

1. Introduction

The sustainable development of our society is confronted with two challenges: fossil resource depletion and waste generation (Coma et al., 2017). The energy supply chain shift towards renewable resources is necessary to create the circular economy (Ranjbari et al., 2022). As a carbon neutral renewable source, biomass has been explored extensively to produce various products relying on co-digestion for bio-wastes valorisation (Avila et al., 2022), chemical looping combustion with CO_2 (Fan et al., 2017), chemical looping gasification (Huang et al., 2017a), simultaneous chemical looping hydrogen production and electricity generation (Mehrpooya et al., 2017). Benefiting from the properties of the inherent CO_2 separation and no NO_x emission, the biomass chemical looping gasification (CLG) based on the chemical looping combustion (CLC) has attracted great attention in syngas production. The fluidized-bed technology was employed to produce H_2 continuously from agricultural biomass with in situ CO_2 capture and sorbent regeneration (Acharya et al., 2009). High CO_2 capture and combustion efficiencies were achieved in 1.5 kWth Chemical looping combustion with oxygen uncoupling (CLOU) unit (Adánez-Rubio et al., 2018). The recent progress of chemical-looping technologies such as gaseous, liquid and solid fuels, and operational experiences were reviewed (Dou et al., 2019; Mattisson et al., 2018; Zhao et al., 2017). CLG circulation system is composed of two separate reactors, fuel reactor and air reactor. The oxygen carrier (OC) is employed to provide the lattice oxygen for the conversion of biomass into syngas in fuel reactor. The reduced oxygen carrier is sent to the air reactor to be oxidized by air to regenerate OC and provide heat. The recent research of biomass CLG has been mainly focused on advances in biomass torrefaction pretreatment (Zhang et al., 2021), biomass and coal co-gasification (Ghosh Ray and Ghangrekar, 2019a; Yan et al., 2018), OC selection and modification (Samprón et al., 2020; Yan et al., 2020), steel industry waste LD Slag as OC (Condori et al., 2021), auto-thermal operation simulation and evaluation (Mohamed et al., 2021; Samprón et al., 2021), biomass chemical looping gasification combined CCS cycle (Mohamed et al., 2020), techno-economic analysis (Aghabararnejad et al., 2015; Jiang et al.,

* Corresponding author.
E-mail address: qinwu@ncepu.edu.cn (W. Qin).

https://doi.org/10.1016/j.indcrop.2022.115544
Received 4 May 2022; Received in revised form 22 August 2022; Accepted 23 August 2022
Available online 30 August 2022

Table 1
The detailed characteristics of the OCs.

OC	Lattice O release capacity	CH_4 conversion	Syngas selectivity	Regeneration gas	Recovery degree	References
CeO_2	46.4	40–55 % (850 ℃)	> 99 %	CO_2/H_2O	82–90%	(Otsuka et al., 1998)
Fe_2TiO_5	200.4	85–90 % (990 ℃)	86–91 %	$CO_2 + O_2$	~100% (O_2 is needed)	(Luo et al., 2014)
Ni-Fe_xO_y	–	> 99 % (900 ℃)	70–80 %	CO_2	~100%	(More and Veser, 2017)
$LaFeO_3$	98.8	69–95 % (850 ℃)	80–90 %	$H_2O + O_2$	> 95% (O_2 is needed)	(Zheng et al., 2017)
Pt-V_2O_3	421.6	80–85 % (850 ℃)	> 99.5 %	CO_2/H_2O	~100%	(Ge et al., 2020b)

Lattice O release capacity: the theoretical CH_4 consumption (mg) per gram OC.

2019) and hydrogen rich syngas production. Biomass gasification is concluded to be more feasible, sustainable, environment-friendly and likely to become competitive with the conventional natural gas reforming method (Udomsirichakorn and Salam, 2014). Biomass CLG may play an important role for renewable hydrogen production in near future.

The waste generation as the second major challenge to our society is expected to jump to 3.4 billion tonnes over the next 30 years by 2050 (Kaza et al., 2018). The waste streams contain a variety of material or compound with energetic or economic value. Driven by brewing and distilling industry, large amount of distillery wastewater also termed stillage, pot ale, slops, or spent wash is produced in fermentation and downstream processes (Song et al., 2020). The distillery wastewater consists of unconvertible organic fractions and high percentage of dissolved organic and inorganic matters with up to 140 g/l chemical oxygen demand and 65 g/l biochemical oxygen demand (Ghosh Ray and Ghangrekar, 2019b). In some cases, ethanol constitutes up to 90 % of the COD content in winery wastewater (Rodriguez-Caballero et al., 2012). From an energy point of view, high concentration of organic compound makes the distillery wastewater suitable for the anaerobic biomethanation production. However, the high chemical stability of phenols, melanoidins, sugar decomposition products of microbial metabolism can be toxic or inhibitory to anaerobic treatment (Phuong and le, Besson, 2019). Therefore, the physico-chemical techniques such as adsorption, nanofiltration, reverse osmosis, flocculation, and oxidation have been also applied for the treatment of the distillery effluents (Ratna et al., 2021). The coupling of the energy intensive CLG and various physico-chemical and biological methods is one of the promising options for distillery wastewater management and value-added compound production. The supercritical water gasification was used to completely remove the pre-drying requirement during H_2 production with empty fruit bunch and palm oil effluent (Ajiwibowo et al., 2019). The syngas composition of chemical looping reforming process with waste cooking oil was determined as a function of reforming temperature (400–1000 °C) (Faleh et al., 2016). 41 kg/h methanol could be produced by integrating hydrothermal treatment and CLC with 100 kg/h municipal solid waste (Hakandai et al., 2022). The high hydrogen concentration in calcium—based CLG could promote the formation of HCl (g) instead of $CuCl_2$ (g), suppressing formation of dioxins in municipal solid waste treatment (Cai et al., 2021).

In this vein, we propose the organic waste chemical looping gasification (OW-CLG) scheme for hydrogen production with the biomass and concentrated distillery wastewater as feedstock. 5% ethanol-containing wastewater was employed for chemical looping reforming using iron-based OC (Qin et al., 2018). It was found that the organic solution (methanol solution) can significantly improve the H_2/CO ratio and η_C in the gasification process compared to water (Qin et al., 2019a, 2019b). The heat released from the OC oxidation can meet heat demand for ethanol reforming reaction, making the whole process exothermic. The organic liquid waste was introduced to activate OC and provide gasification agent of CLG for H_2 production (Zheng et al., 2020a). The simultaneous modification of Fe_2O_3/Al_2O_3 and supplement of oxidant for biomass CLG by introducing KNO_3 containing ethanol liquid waste indicated that the alkaline organic liquid waste could boost solid fuel gasification (Qin et al., 2021). It was found that methane accounted for the composition of syngas up to 11.2 % (Zheng et al., 2020b). Although 12.5% CH_4 addition as diluent in syngas results in no change in CO conversion during Fischer-Tropsch synthesis and relaxing the purification process for complete CH_4 removal (Badoga et al., 2017), the reforming of syngas is necessary for the sake of high yield hydrogen production. Methane feedstock is consumed to provide heat for the conventional steam reforming of natural gas, leading to only 76% yield of product energy (Krenzke et al., 2017). The chemical looping reforming (CLR) of methane via metal oxide redox cycle is a promising approach to hydrogen production (Chuayboon et al., 2020). Various metal oxides including CeO_2, Fe_2TiO_5, Ni-Fe_xO_y, $LaFeO_3$, Pt-V_2O_3 are particularly attractive candidate due to their physical and chemical properties (shown in Table 1). Compared with other oxygen carrier, V_2O_3 and CeO_2 have the comparable high selectivity to CO. But CeO_2 catalysis activity of methane conversion is only 40–55 % (850 ℃), while Fe_2TiO_5, Ni-Fe_xO_y, $LaFeO_3$ have the low lattice O release capacity of 46.4–200.4. V_2O_3 exhibits good performances in CH_4 conversion rate, CO_2 oxidation regeneration, high lattice oxygen storage capacity, redox stability, and high selectivity to H_2 and CO. It was found that the CH_4

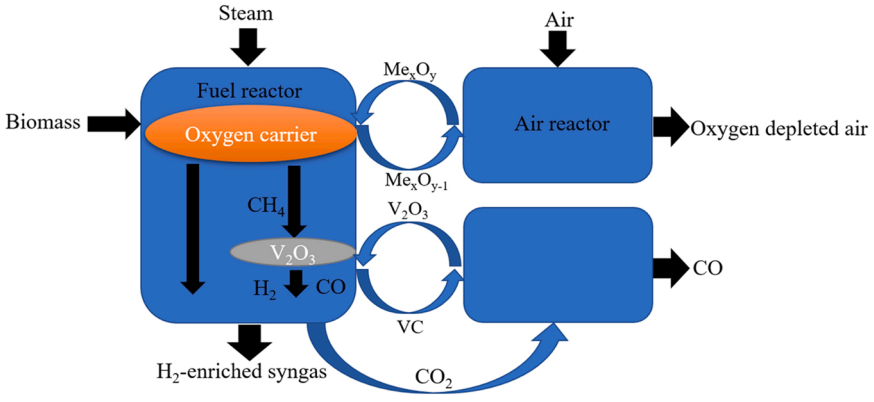

Fig. 1. OW-CLG for hydrogen production.

Table 2
Proximate analysis and ultimate analysis of the corn stalk.

As received (ar)		
Proximate analysis (wt%)	Volatile (V_{ar})	67.42
	Fixed carbon (F_{ar})	12.94
	Ash (A_{ar})	9.35
	Moisture (M_{ar})	10.29
Ultimate analysis (wt%)	Carbon (C_{ar})	41.14
	Hydrogen (H_{ar})	5.94
	Nitrogen (N_{ar})	0.58
	Oxygen (O_{ar})	32.54
	Sulfur (S_{ar})	0.17

conversion of pristine V_2O_3 is less than 50% and the CH_4 conversion of Pt-V_2O_3 during cycling reached 81.7 % (Ge et al., 2020a).

In this regard, OW-CLG and CLR are combined in this work to produce hydrogen with corn stalks and distillery wastewater (shown in Fig. 1). The ethanol solution is used as model distillery wastewater to provide sufficient steam and organic compound. V_2O_3 is employed as CLR metal oxide to reform CH_4 into H_2 and CO. The reduced V_2O_3 can be regenerated by CO_2 separated from the syngas.

To this end, Hydrogen production by organic waste chemical looping gasification (OW-CLG) enhanced by V_2O_3 catalyzed reforming via partial oxidation approach were investigated with biomass and ethanol solution. The effect of reaction condition on CH_4 conversion and hydrogen production was determined in detail. The kinetic and thermodynamic analysis were further conducted to reveal the reaction characteristics and feasibility of the OW-CLG process.

2. Methods

2.1. Materials

The corn stalks and ethanol solution (6% volume fraction) were used as the feedstocks for OW-CLG system. OC of the Fe_2O_3/Al_2O_3 containing 40 wt% Al_2O_3 and 60 wt% Fe_2O_3 was prepared by the impregnation method (Adánez-Rubio et al., 2018). Al_2O_3 powder was added to saturated $Fe(NO_3)_3$ solution. The mixture was stirred at 70 °C until it become paste. After drying at 100 °C, the mixture was then calcined in the muffle furnace for 1.5 h at 900 °C. The prepared Fe_2O_3/Al_2O_3 was ground into 60–80 mesh OC powder. The proximate analysis and ultimate analysis of the corn stalk were conducted (shown in Table 2). The molecular formula could be determined as $C_{1.7}H_3O$.

2.2. Experiment and analysis

As shown in Fig. 1, the OW-CLG experimental system includes a gas flow control system, a quartz tube with an inner diameter of 18 mm and a height of 900 mm, a gas chromatograph (Agilent 490Micro GC), an injection pump, a condensation and drying system, and a vertical tube furnace. V_2O_3 was added to a quartz reaction tube in advance. N_2 flow with a rate of 160 ml/min was controlled by a mass flow meter to maintain the inert atmosphere. The mixture of corn stalks and OC was poured on the quartz wool fixed in the reactor when the reactor in the electric furnace was heated to the predetermined reaction temperature. 10 ml of 6 % ethanol solution was injected into the reactor at a constant rate within 30 min using the injection pump. Gas products were analyzed by an online gas chromatograph every 5 min.Fig. 2.

2.3. Data evaluation

The flow rate of outlet gas (q_t) during the experiment was calculated as

$$q_t = \frac{q_{N_2}}{1 - \sum x_i} \tag{1}$$

where q_{N_2} is the inlet N_2 flow rate (ml/min), x_i is volume fraction of H_2, CO, CH_4, CO_2 in the outlet gas respectively.

The real flow rates of various outlet gas components were calculated as

$$q_i(t) = q_t \times x_i \tag{2}$$

where $q_i(t)$ is the real flow rates of various outlet gas component, x_i is volume fraction of H_2, CO, CH_4, or CO_2 in the outlet gas.

The total volume of various outlet gas was calculated as

$$Q_i = \int q_i(t)dt \tag{3}$$

where Q_i is the total volume of various outlet gas component, $q_i(t)$ is the

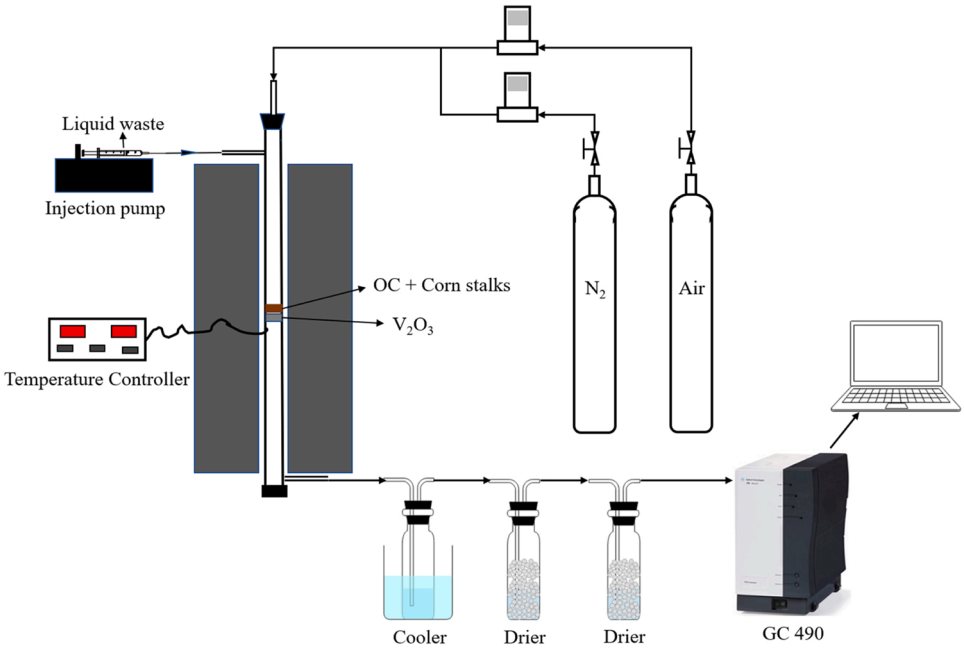

Fig. 2. Schematic diagram of OW-CLG experiment process.

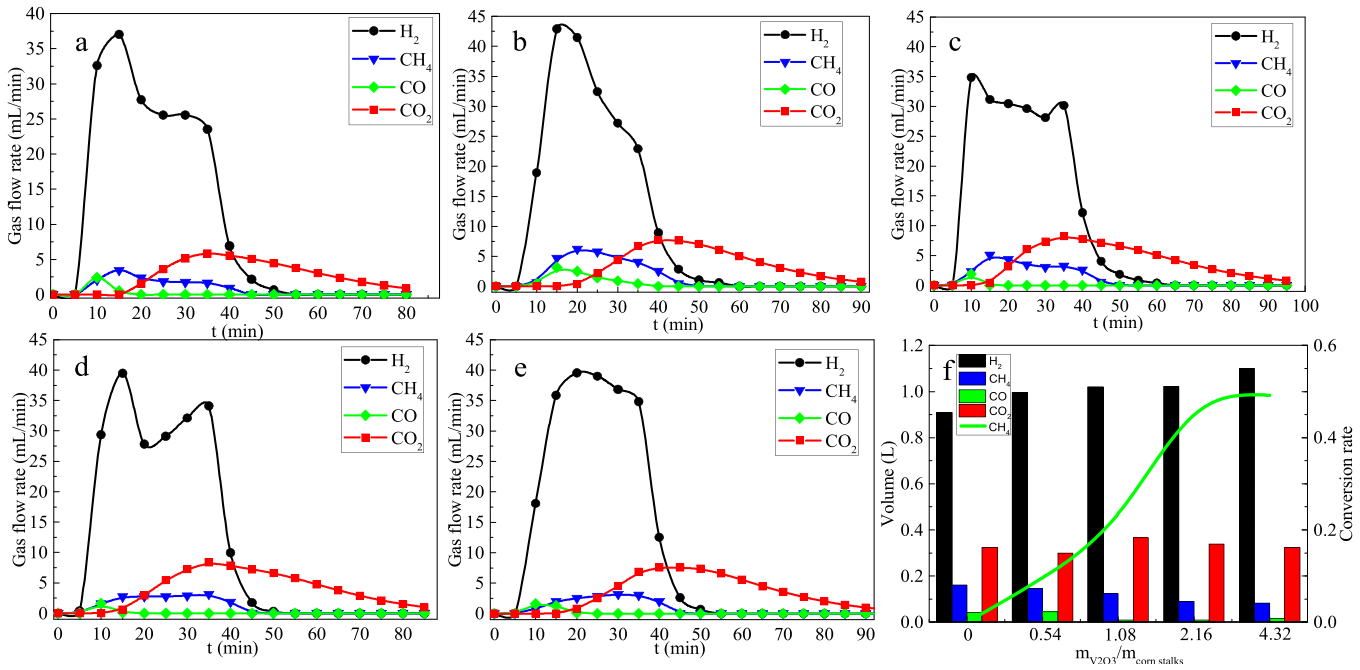

Fig. 3. Effect of mass ratio of V_2O_3 on corn stalk gasification.

real flow rates of various outlet gas component.

Carbon conversion rate (η_C) could be calculated based the molar ratio of carbon in outlet gas to carbon in fuel feedstock

$$\eta_C = \frac{24.45\left(Q_{CO} + Q_{CH_4} + Q_{CO_2}\right)}{\left(n_{fuel}\right)} \tag{4}$$

where η_C is Carbon conversion rate, Q_{CO}, Q_{CH_4}, Q_{CO_2} are the total volume of CO, CH_4, and CO_2 in outlet gas, n_{fuel} is the molar ratio of carbon in fuel feedstock.

CH_4 conversion rate was defined as

$$CH_4\text{conversion} = 1 - Q^0_{CH4} \tag{5}$$

where Q_{CH_4} is the total volume of CH_4 in outlet gas, $Q^0_{CH_4}$ is the total volume of CH_4 in the experiment without adding V_2O_3.

Cold gas efficiency (η_{CGE}) could be calculated as

$$\eta_{CGE} = \frac{q_{H_2} + q_{CH_4} + q_{CO}}{q_{fuel}} \tag{6}$$

where q_{fuel} is the total calorific value of the fuel in the gasifier, q_x is the total calorific value of outlet gas component x.

Oxygen excess ratio (Ω), defined as the ratio of oxygen provided by OC to the oxygen required for the complete combustion of the biomass, could be obtained according to the method mentioned in the previous work (Huang et al., 2014).

3. Results and discussion

3.1. Gasification reaction characteristics under various mass ratio of V2O3 to corn stalk

The reduction mechanism of Fe_2O_3 during gasification is very complicated. Normally it undergoes a sequential pathway for the variation in oxidation of state from "+ 3" to 0. The H_2 production was enhanced by adding waste liquid vapor into reaction system at Ω of 0.2 as in R6 (Fan, 2010; Kale et al., 2013). CO is easily oxidized by OC (R9), and water–gas shift reaction (R10) is the equilibrium-limited reaction at higher temperatures (Prasad and Kuester, 1988). Therefore, CO remains at a low level during gasification. When $\Omega > 0.2$, the rate of R8 is higher than that of hydrogen production reaction, resulting in a decrease in hydrogen production (More and Veser, 2017; Zeng et al., 2016). Therefore, the effect of various $m_{V_2O_3}/m_{corn\ stalk}$ (ranging from 0 to 4.32) on OW-CLG was investigated at Ω and temperature of 0.2 and 700 °C. The total volume and real flow rates of various outlet gas are shown in Fig. 3. The highest CH_4 conversion rate of 49.2 % was observed at $m_{V_2O_3}/m_{corn\ stalk}$ of 4.32 (shown in Fig. 3f). The plausible explanation may reside in that high $m_{V_2O_3}/m_{corn\ stalk}$ is conducive to CH_4 reforming reaction (R12), promoting the decomposition of CH_4 (Ge et al., 2020b). The flow rate of H_2 increased significantly in the initial stage due to steam reforming reaction (R2~R6) (de Vos et al., 2019; Kale et al., 2013). The outlet gas is mainly composed of CO_2 and H_2 within the first 30 min of the reaction, as well as a certain amount of CH_4 produced by the pyrolysis of biomass and ethanol (R1).

$$C_{1.7}H_3O + CH_3CH_2OH \rightarrow H_2 + CO + C_nH_m + CO_2 + C + \text{char} + H_2O \quad \text{(R1)}$$

$$H_2O + C/\ \text{char} \rightarrow H_2 + CO\ /\ CO_2 \quad \text{(R2)}$$

$$2\ H_2O + C \rightarrow 2\ H_2 + CO_2 \quad \text{(R3)}$$

$$CH_3CH_2OH + Fe_2O_3 + H_2O \rightarrow CO\ /\ CO_2 + H_2 + (CH_4) + Fe_2O_{3-x} \quad \text{(R4)}$$

$$C_6H_{10}O_5 + Fe_2O_3 + H_2O \rightarrow CO\ /\ CO_2 + H_2 + (CH_4) + Fe_2O_{3-x} \quad \text{(R5)}$$

$$Fe_2O_{3-x} + H_2O \rightarrow Fe_3O_4 + H_2 \quad \text{(R6)}$$

$$CH_4 + Fe_2O_3 \rightarrow CO_2 + H_2O + Fe_2O_{3-x} \quad \text{(R7)}$$

$$H_2 + Fe_2O_3 \rightarrow H_2O + Fe_2O_{3-x} \quad \text{(R8)}$$

$$CO + Fe_2O_3 \rightarrow CO_2 + Fe_2O_{3-x} \quad \text{(R9)}$$

$$CO + H_2O \rightarrow CO_2 + H_2 \quad \text{(R10)}$$

$$CH_4 + H_2O \rightarrow H_2 + CO \quad \text{(R11)}$$

$$CH_4 + V_2O_3 \rightarrow H_2 + CO + VC \quad \text{(R12)}$$

Compared with the control, CH_4 conversion (R12) was favored with increasing $m_{V_2O_3}/m_{corn\ stalk}$, which is beneficial for H_2 production. CO content of the outlet gas is low even CH_4 is decomposed in this work, which is consistent with the previous result (Prasad and Kuester, 1988).

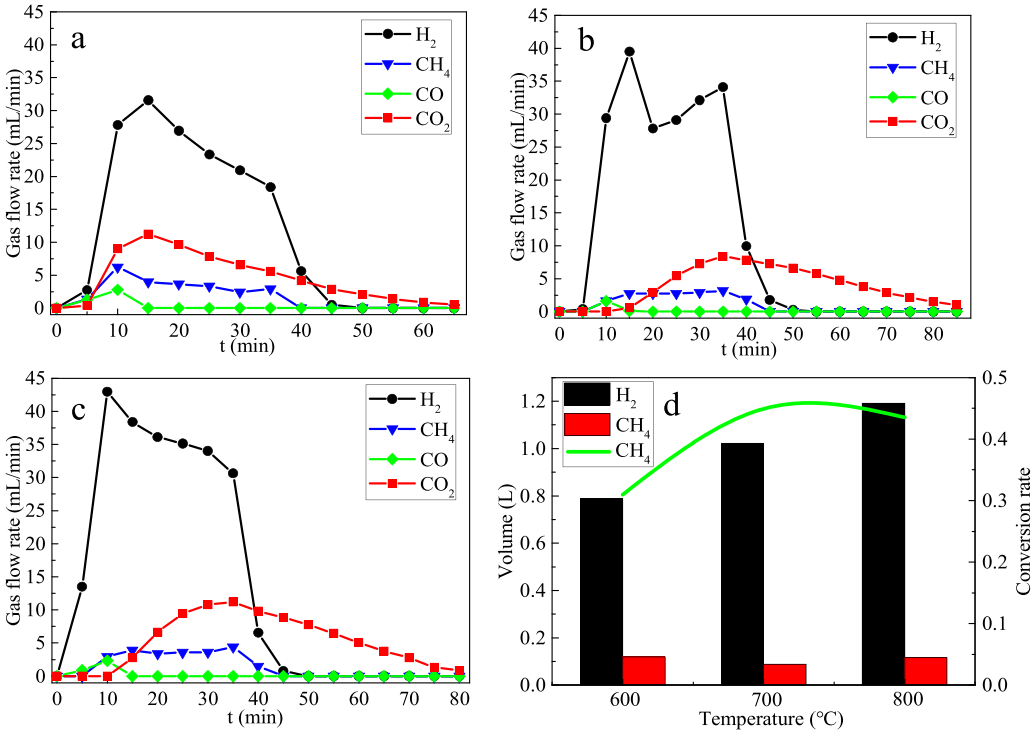

Fig. 4. Effect of temperature on the corn stalks gasification.

Along with the increase of $m_{V_2O_3}/m_{corn\ stalk}$ from 4 to 8, only slight increase of CH_4 conversion rate was detected (from 44.9 % to 49.2 %). When the $m_{V_2O_3}/m_{corn\ stalk}$ is 2.16, the optimal reaction conditions for CH_4 conversion can be obtained.

a-e: the volume flow rate of various gases in the outlet gas at 0, 0.54, 1.08, 2.16, 4.32; f: the effect of $m_{V_2O_3}/m_{corn\ stalk}$ on the total volume of various gases and CH_4 conversion rate at Ω and temperature of 0.2 and 700 °C.

3.2. Gasification reaction characteristics under different temperature

The effect of temperature on the corn stalks CLG was investigated at Ω and $m_{V_2O_3}/m_{corn\ stalk}$ of 0.2 and 2.16. As shown in Fig. 4, the highest CH_4 conversion rate was detected at 700 ℃. The total hydrogen production increased with the increasing temperature. The activity of the OC and V_2O_3 are greatly improved at higher temperature. It was found at R3, R10, R11 (Al-Zareer et al., 2018; Qin et al., 2015; Shen et al., 2008) dominate the conversion reaction (Franco et al., 2003), and the oxidation state of the reduced OC is also more efficient than the OC consumption process (Inayat et al., 2010), such as R6 (Huang et al., 2017b), making the H_2 production rate higher than H_2 consumption rate. In addition, since R11 is an endothermic reaction (Zaini et al., 2017), methane reforming to produce more H_2 is conducive at high temperature. The activity of the V_2O_3 is low at 600 ℃, leading to low CH_4 conversion rate. When the temperature increased to 800 ℃, the hydrogen production is further enhanced. What should be mentioned is the CH_4 conversion rate tends to decrease when temperature was further raised from 700 ℃ to 800 ℃. As shown in Fig. 4d, the H_2 output amounts up to 1.02 L at 700 ℃. The low temperature is not conducive to the activity of the OC and conversion reaction. The high temperature could promote the hydrogen production reaction and but has little effect on the promotion of CH_4 conversion reaction. The highest CH_4 conversion rate of 44.9 % can be obtained under the condition of $m_{V_2O_3}/m_{corn\ stalk}$, Ω, and temperature *of* 2.16, 0.2 700 °C.

a-c: the volume flow rate of various gases in the outlet gas at 600, 700, 800 ℃; d: the effect of temperature on the total volume of various gases and CH_4 conversion rate at Ω and $m_{V_2O_3}/m_{corn\ stalk}$ of 0.2 and 2.16.

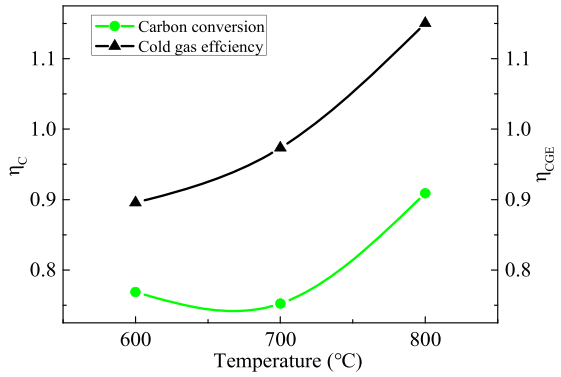

Fig. 5. Effect of temperature on carbon conversion and cold gas efficiency of the corn stalks gasification.

As shown in Fig. 5, high temperature is beneficial to improving carbon conversion rate and cold gas efficiency during corn stalks gasification. At 800 °C, the cold gas efficiency of corn stalks gasification is higher than 1, which is attributed to the fact that water vapor would oxidize the reduced OC to generate a large amount of H_2, resulting in an increase in the calorific value of the gas produced.

3.3. Kinetics analysis

Kinetics of OW-CLG was analyzed at the optimal temperature, Ω and $m_{V_2O_3}/m_{corn\ stalk}$ of 700 °C, 0.2 and 2.16 respectively. The total volume of carbon-containing gas (Q_C) is calculated based on the integral calculation of Q_{CH_4}, Q_{CO} and Q_{CO_2} as

$$Q_C = Q_{CH_4} + Q_{CO} + Q_{CO_2} \quad (7)$$

The molar amount of carbon conversion (n_C) in the OW-CLG process could be expressed as

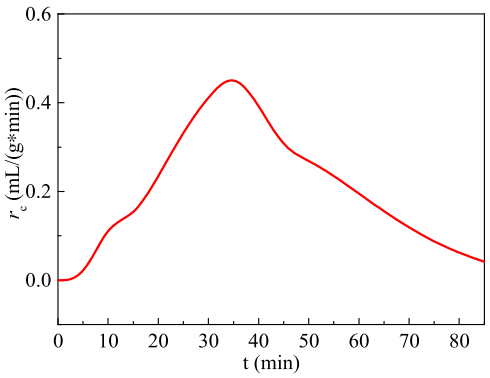

Fig. 6. The calculated r_c for OW-CLG process under $\Omega = 0.2$, $T = 700$ °C, and $m_{V_2O_3}/m_{corn\ stalk} = 2.16$.

$$n_C = \frac{Q_C}{24.45} \tag{8}$$

The carbon conversion rate (r_c)was calculated as

$$r_c = \frac{dn_c}{m_{oc}dt} \tag{9}$$

where m_{oc} is the mass of the used OC (Fe2O3/Al2O3).

The r_c curve at the optimal was depicted in Fig. 6. The carbon conversion rate increased gradually during liquid waste addition in the initial 35 min, which indicated that the pyrolysis of CH_3CH_2OH and corn stalks was promoted to produce CO, CO_2, H_2, H_2O, hydrocarbons (C_nH_m), tar and coke (R1) when the waste liquid was introduced. CH_3CH_2OH, corn stalks and C_nH_m are partially oxidized by Fe_2O_3 to CO, CO_2 and H_2 (R4, R5). Meanwhile, the introduction of water vapor promotes the conversion of tar and coke, accompanied by the generation of CO, CO_2 and H_2 (R2, R3). The peak value of 0.472 ml/(g•min) was obtained at 35 min r_c keeps decreasing after the addition of ethanol solution in the batch gasification process, which confirmed that the increase and subsequent decrease of r_c was mainly caused by the reactions R2-R4 and the depletion of water vapor (Guo et al., 2015). In the first 35 min, the production of syngas or hydrogen is mainly the result of steam reforming and ethanol decomposition reactions (R2-R4, R6) (Najera et al., 2011), rather than the direct partial oxidation of corn stalks by lattice oxygen. The remaining fixed carbon hardly contributes to conversion to syngas.

3.4. Thermal dynamics analysis

Based on the Doml3 module in the Material Studio software, the Gibbs free energies of some of these reactions can be calculated. The formula for calculating the data processing is as follows:

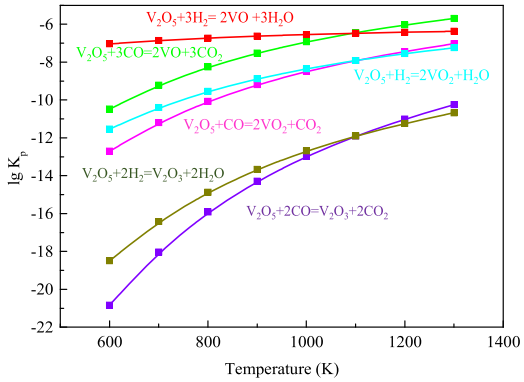

Fig. 8. Relation between K_p and temperature in redox reactions of vanadium in various oxidation states.

$$E^T_{Tcorr} = E_{total} + G_{total} \tag{10}$$

$$\Delta G^T_{reaction} = E^T_{Tcorr}(Product) - E^T_{Tcorr}(Reactant) \tag{11}$$

The total energy (E^T_{Tcorr}) used to calculate the Gibbs free energy includes the total energy of the model and the finite temperature corrections for the standard thermodynamic quantities. All these quantities include the zero-point vibrational energy (ZPVE). The reaction equilibrium constant (K_p) can be calculated as follows:

$$InK_p = \frac{\Delta G}{RT} \tag{12}$$

$$lgK_p^{1000K} = lg\frac{P^2_{CO}}{P^2_{CO_2}} = -5.97 \tag{13}$$

$$lgK_p^{1000K} = lg\frac{P^2_{H_2}}{P^2_{H_2O}} = -12.69 \tag{14}$$

where ΔG, R, T, and P_X are the Gibbs free energy, thermodynamic constant, temperature, and partial pressure of component X, respectively. The variation trend of ΔG with temperature in the redox reactions of various vanadium compounds is shown in Fig. 7. The relationship between the K_p of the redox reaction of vanadium in each oxidation state and the temperature is shown in Fig. 8.

$$V_2O_5 + 3H_2 \rightarrow 2VO + 3H_2O \tag{R13}$$

$$V_2O_5 + 3CO \rightarrow 2VO + 3CO_2 \tag{R14}$$

$$V_2O_5 + H_2 \rightarrow 2VO_2 + H_2O \tag{R15}$$

$$V_2O_5 + CO \rightarrow 2VO_2 + CO_2 \tag{R16}$$

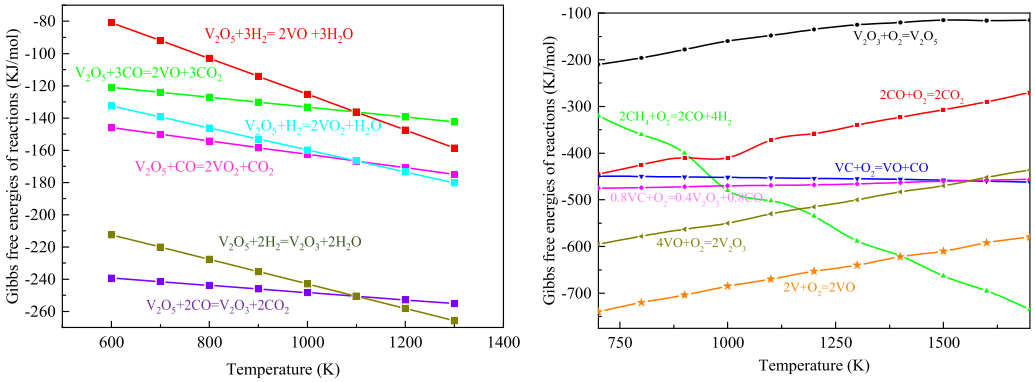

Fig. 7. Relationship between ΔG and temperature in redox reactions of vanadium in various oxidation states.

$$V_2O_5 + 2H_2 \rightarrow V_2O_3 + 2H_2O \quad \text{(R17)}$$

$$V_2O_5 + 2CO \rightarrow V_2O_3 + 2CO_2 \quad \text{(R18)}$$

$$V_2O_3 + O_2 \rightarrow V_2O_5 \quad \text{(R19)}$$

$$2CH_4 + O_2 \rightarrow 2CO + 4H_2 \quad \text{(R20)}$$

$$2CO + O_2 \rightarrow 2CO_2 \quad \text{(R21)}$$

$$VC + O_2 \rightarrow CO + VO \quad \text{(R22)}$$

$$0.8VC + O_2 \rightarrow 0.4V_2O_3 + 0.8CO \quad \text{(R23)}$$

$$4VO + O_2 \rightarrow 2V_2O_3 \quad \text{(R24)}$$

$$2V + O_2 \rightarrow 2VO \quad \text{(R25)}$$

$$2VC + 5CO_2 \rightarrow V_2O_3 + 7CO \quad \text{(R26)}$$

The thermodynamic properties of V_2O_3 in the catalytic reforming of CH_4 can be evaluated by the ΔG versus temperature. Since vanadium has various oxidation states, such as redox pairs such as V_2O_5-VO_2, V_2O_5-V_2O_3, V_2O_5-VO, V_2O_5-V_2O_3, V_2O_3-VO, VO-V, V_2O_3-VC, and VO-VC, it can be predicted from Fig. 7 the possible pathways of V_2O_3 during the preparation and redox reactions process. Fig. 8 shows the thermodynamic possibility of reducing V_2O_5 to V_2O_3 using H_2 during V_2O_3 preparation (R17), but the reduced V_2O_3 cannot be regenerated at high temperature in the presence of air because the reduced V_2O_3 may be oxidized to V_2O_5 and lose the ability to catalyze CH_4 reforming to produce hydrogen (R19). The excellent catalytic performance of V_2O_3 for methane reforming has been demonstrated (Ge et al., 2020b). The thermodynamically feasible temperature range for the partial oxidation of CH_4 to hydrogen by V_2O_3 (R20) is above 950 K, which explains the low CH_4 conversion at low temperature (600 °C). The reduced V_2O_3 can be oxidized and regenerated into V_2O_3 by CO at 750–1500 K, which confirms the low CO content in the syngas after adding V_2O_3. And the excess V_2O_3 will not further oxidize CO to CO_2. The R27-R30 reactions are thermodynamically difficult to proceed in 800–1300 K. Equations (28) and (29) show that H_2O and CO_2 components account for a large proportion in the corresponding reactions at 1000 K, indicating that V_2O_3 is difficult to react with H_2O and CO_2, and V_2O_3 mainly partially oxidizes CH_4. However, at 1000 K, it is thermodynamically feasible for V_2O_3 to oxidize H_2 to generate H_2O. Therefore, excessive addition of V_2O_3 may lead to the oxidation of H_2, resulting in a decrease in H_2 production. In addition, the reaction of V_2O_3 and VO with CH_4 is thermodynamically feasible in 800–1000 °C, while the reduction of VO to elemental vanadium can only proceed above 1200 °C. The sum of the reaction R20 and R23 is equal to the reaction R12, so V_2O_3-VC is the overall redox pair of the V_2O_3 OC in 950–1300 K. The regeneration process of V_2O_3 OC during OW-CLG proceeds through reaction R26.

$$V_2O_3 + 2H_2O \rightarrow V_2O_5 + 2H_2 \quad \Delta G > 0 \quad \text{(R27)}$$

$$V_2O_3 + H_2O \rightarrow 2VO_2 + H_2 \quad \Delta G > 0 \quad \text{(R28)}$$

$$V_2O_3 + 2CO_2 \rightarrow V_2O_5 + 2CO \quad \Delta G > 0 \quad \text{(R29)}$$

$$V_2O_3 + CO_2 \rightarrow 2VO_2 + CO \quad \Delta G > 0 \quad \text{(R30)}$$

Analysis of the OW-CLG thermal conversion process is crucial for evaluating whether the system can operate stably. the corn stalk OW-CLG can obtain higher H_2 yield and CH_4 conversion rate at temperature, $m_{V_2O_3}/m_{corn\ stalk}$ and Ω of 700 ℃, 2.16, and 0.2. Therefore, under this optimal reaction condition, the thermodynamic analysis of the OW-CLG process is carried out. Based on the electron balance, the average valence of iron after reduction is 2.02, the molecular formula of reduced iron oxide can be approximated as $Fe_2O_{2.02}$ (Ge et al., 2020b). The reaction process formula of corn stalk OW-CLG is as follows:

$$1.8C_{1.7}H_3O + 1.5C_2H_6O + 1.7Fe_2O_3 + 5.1H_2O \rightarrow 11.3H_2 + CH_4 + 0.1CO + 5CO_2 + 1.7Fe_2O_{2.02} \quad \text{(R31)}$$

Table 3
Thermodynamic parameters for various components.

	$\Delta_r H_m^\theta$ (298.15 K, kJ/mol)	$C_{m,p}$ (J/ (mol·K))
Fe_2O_3	-824.2	$C_p = 6.8279 + 0.4689–0.0006\ T^2 + 3 \times 10^{-7}\ T^3$
FeO	-272	$C_p = 44.711 + 0.0195\ T\text{-}5 \times 10^{-6}\ T^2$
Fe_3O_4	-1118.4	$C_p = 104.2096 + 0.4689\ T + 178.5108\ T^2 + 10.61510\ T^3$
C_2H_6O	-235.1	$C_p = 29.25 + 166.28 \times 10^{-3} \times T\text{-}48.898 \times 10^{-6} \times T^2$
CO_2	-393.509	$C_p = 26.75 + 42.258 \times 10^{-3} \times T\text{-}14.25 \times 10^{-6} \times T^2$
CO	-110.525	$C_p = 26.537 + 7.6831 \times 10^{-3} \times T\text{-}1.172 \times 10^{-6} \times T^2$
CH_4	-74.81	$C_p = 14.15 + 75.496 \times 10^{-3} \times T\text{-}17.99 \times 10^{-6} \times T^2$
H_2O	-241.818	$C_p = 30 + 10.7 \times 10^{-3} \times T\text{-}2.022 \times 10^{-6} \times T^2$
Fe	0	$C_p = 0.45 \times 10^3$
O_2	0	$C_p = 36.16 + 0.845 \times 10^{-3} \times T\text{-}0.7494 \times 10^{-6} \times T^2$

$C_{m,p}$: molar isobaric hot melt.
$\Delta_r H_m^\theta$: standard molar reaction enthalpy.

According to the thermodynamic parameters in Table 3, the enthalpy of the R31 can be calculated, $\Delta H_{mol} = 1049.391$ kJ/mol. The corn stalk OW-CLG is an endothermic process, and the total endothermic heat is 4.237 kJ. 0.021 mol H_2O is evaporated, and the heat absorbed by evaporation is 0.903 kJ, while 0.006 mol ethanol is evaporated, and the heat absorbed by evaporation is 0.256 kJ. During this process, OC can not only transfer lattice oxygen but also act as a heat carrier (Qin et al., 2019a, 2019b) to transfer the heat between FR and AR. In the AR, the OC oxidation regeneration process equation is as follows:

$$FeO + 0.25O_2 \rightarrow 0.5Fe_2O_3 \Delta H_{mol} = -127.768 kJ/mol \quad \text{(R32)}$$

$$Fe + \quad 0.75O_2 \rightarrow 0.5Fe_2O_3 \Delta H_{mol} = -753.739 kJ/mol \quad \text{(R33)}$$

According to the calculation results, the corn stalk OW-CLG process needs to absorb 5.396 kJ of heat. In the AR, the oxidation reaction of the reduced OC releases 2.913 kJ of heat. The heat released by the oxidation of the reduced OC can't meet the heat required for the corn stalk OW-CLG process, which means that external supplementary heat is required to maintain the entire corn stalk OW-CLG process.

3.5. Structural characterizations

The characterizations of the fresh OC ($Fe_2O_3/A1_2O_3$) have been performed previously via scanning electron microscopy (SEM), X-ray diffraction (XRD) *etc*. The diffraction peaks in the XRD pattern of the fresh OC correspond to the different crystalline phases of Fe_2O_3 and there is no $A1_2O_3$ diffraction peak, indicating that the prepared OC has high crystallinity and Fe_2O_3 has good coverage on the surface of $A1_2O_3$ (Luo et al., 2021; Zheng et al., 2020a). The SEM image shows that the fresh oxygen carrier has smooth surface and good porosity, which is conducive to the gasification intermediate product to penetrate into the OC particles and improve its reaction activity. In addition, the good cycle characteristic of OCs based on Fe_2O_3 have been verified (Qin et al., 2019a and 2019b, 2015).

As shown in Fig. 9, the surface particles of fresh V_2O_3-based OC are evenly distributed and have high porosity, which is conducive to the penetration of gasification intermediate products into the interior of the V_2O_3-based OC particles. After reduction at 700 °C, the uniform surface

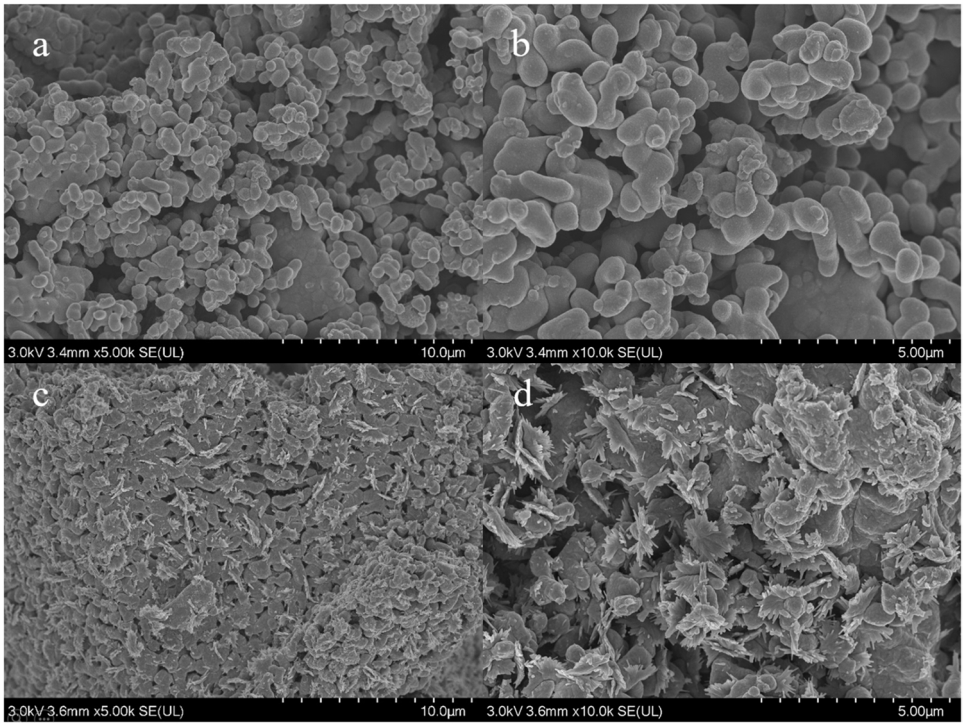

Fig. 9. SEM images (a-b) for the fresh V_2O_3 and (c-d) for the V_2O_3 after reaction.

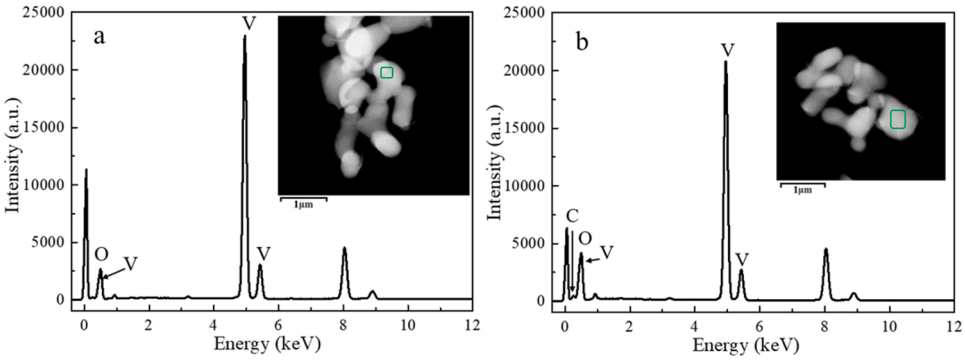

Fig. 10. Transmission electron microscope - Energy dispersive spectrometer (TEM – EDS) of V_2O_3 before a) and after b) reaction.

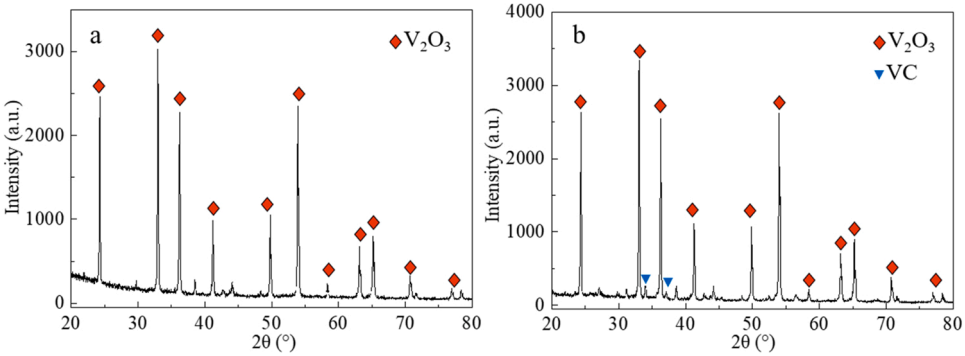

Fig. 11. XRD patterns of V_2O_3 before a) and after b) reaction.

and pores of the V_2O_3-based OC particles are destroyed, small fragments aggregate into clusters, leading to the decrease in surface porosity. In addition, after the reforming of CH_4, carbon deposits may form on the surface of V_2O_3-based OC, clogging the pores of OC. Many small pores are re-formed on the surface of the reduced V_2O_3-based OC in Fig. 9d, which can be attributed to the gas flowing between V_2O_3-based OC particles. From Fig. 10, the reacted V_2O_3-based OC contains 1.46%wt C. As shown in Fig. 11, the XRD peak indicates that the final reduction state

of V_2O_3 is the VC phase. The fewer peaks corresponding to VC after the reaction may be attributed to the oxidation of VC to V_2O_3 by CO_2 in the synthesis gas (Ge et al., 2020b), which also verifies the V_2O_3-VC redox pair for V_2O_3-based OC.

4. Conclusions

The organic waste chemical looping gasification (OW-CLG) scheme for hydrogen production with the biomass and concentrated distillery wastewater as feedstock was proposed in this work. V_2O_3 was employed to promote methane reforming to improve the efficiency of hydrogen production by partially oxidation. Compared with the control, the optimal methane conversion rate of 44.9% is obtained at Ω, temperature, and $m_{V_2O_3}/m_{corn\ stalk}$ of 0.2, 700 ℃, and 2.16. The highest H_2 yield is 2.05 l with 1 g corn stalk and 20 ml ethanol model solution. Combined with the analysis of kinetics and thermodynamics, it was verified that the introduction of distillery wastewater and V_2O_3 could promote hydrogen production in the OW-CLG process. The novel OW-CLG strategy can reduce the energy consumed for separating CH_4 while processing ethanol liquid waste.

CRediT authorship contribution statement

Zongming Zheng: Writing – original draft, Visualization, Conceptualization. **Laixing Luo:** Conceptualization, Methodology, Software, Formal analysis, Data curation. **Xing Zheng:** Methodology, Software, Formal analysis, Data curation. **Ruonan Duan:** Writing – original draft, Visualization. **Xianbin Xiao:** Validation, Writing – review & editing, Supervision, Project administration, Funding acquisition. **Changqing Dong:** Language. **Wu QIN:** Investigation, Resources.

Declaration of Competing Interest

The authors declare that they have no known competing financial interests or personal relationships that could have appeared to influence the work reported in this paper.

Data Availability

Data will be made available on request.

Acknowledgments

The authors wish to thank the National Key Research and Development Program of China (2021YFE0194500), the National Natural Science Foundation of China (32171915), the Fundamental Research Funds for the Central Universities (2018ZD08).

References

Acharya, B., Dutta, A., Basu, P., 2009. Chemical-looping gasification of biomass for hydrogen-enriched gas. Energy Fuels 23. https://doi.org/10.1021/ef9003889.

Adánez-Rubio, I., Pérez-Astray, A., Mendiara, T., Izquierdo, M.T., Abad, A., Gayán, P., de Diego, L.F., García-Labiano, F., Adánez, J., 2018. Chemical looping combustion of biomass: CLOU experiments with a Cu-Mn mixed oxide. Fuel Process. Technol. 172. https://doi.org/10.1016/j.fuproc.2017.12.010.

Aghabararnejad, M., Patience, G.S., Chaouki, J., 2015. Techno-economic comparison of a 7-MWth biomass chemical looping gasification unit with conventional systems. Chem. Eng. Technol. 38. https://doi.org/10.1002/ceat.201400503.

Ajiwibowo, M.W., Darmawan, A., Aziz, M., 2019. Towards clean palm oil processing: Integrated ammonia production from empty fruit bunch and palm oil effluent. J. Clean. Prod. 236. https://doi.org/10.1016/j.jclepro.2019.117680.

Al-Zareer, M., Dincer, I., Rosen, M.A., 2018. Analysis and assessment of a hydrogen production plant consisting of coal gasification, thermochemical water decomposition and hydrogen compression systems. Energy Convers. Manag. 157. https://doi.org/10.1016/j.enconman.2017.11.047.

Avila, R., Justo, Á., Carrero, E., Crivillés, E., Vicent, T., Blánquez, P., 2022. Water resource recovery coupling microalgae wastewater treatment and sludge co-digestion for bio-wastes valorisation at industrial pilot-scale. Bioresour. Technol. 343. https://doi.org/10.1016/j.biortech.2021.126080.

Badoga, S., Sohani, K., Zheng, Y., Dalai, A.K., 2017. Mesoporous alumina and alumina-titania supported KCuFe catalyst for Fischer-Tropsch synthesis: Effects of CO_2 and CH4 present in syngas. Fuel Process. Technol. 168. https://doi.org/10.1016/j.fuproc.2017.08.033.

Cai, J., Zheng, W., Luo, M., Kuang, C., Tang, X., 2021. Characterization of copper (II) chemical forms and heavy metal distribution in chemical looping gasification of municipal solid waste. J. Energy Inst. 96. https://doi.org/10.1016/j.joei.2021.03.005.

Chuayboon, S., Abanades, S., Rodat, S., 2020. High-purity and clean syngas and hydrogen production from two-step CH4 reforming and H2O splitting through isothermal ceria redox cycle using concentrated sunlight. Front. Energy Res. 8. https://doi.org/10.3389/fenrg.2020.00128.

Coma, M., Martinez-Hernandez, E., Abeln, F., Raikova, S., Donnelly, J., Arnot, T.C., Allen, M.J., Hong, D.D., Chuck, C.J., 2017. Organic waste as a sustainable feedstock for platform chemicals. https://doi.org/10.1039/c7fd00070g.

Condori, O., García-Labiano, F., de Diego, L.F., Izquierdo, M.T., Abad, A., Adánez, J., 2021. Biomass chemical looping gasification for syngas production using LD Slag as oxygen carrier in a 1.5 kWth unit. Fuel Process. Technol. 222. https://doi.org/10.1016/j.fuproc.2021.106963.

Dou, B., Zhang, H., Song, Y., Zhao, L., Jiang, B., He, M., Ruan, C., Chen, H., Xu, Y., 2019. Hydrogen production from the thermochemical conversion of biomass: Issues and challenges. Sustain. Energy Fuels. https://doi.org/10.1039/c8se00535d.

Faleh, N., Hajjaji, N., Pons, M.N., 2016. Thermodynamic investigation of waste cooking oil based hydrogen generation system with chemical looping process. South Afr. J. Chem. Eng. 21. https://doi.org/10.1016/j.sajce.2016.04.001.

Fan, J., Hong, H., Zhu, L., Jiang, Q., Jin, H., 2017. Thermodynamic and environmental evaluation of biomass and coal co-fuelled gasification chemical looping combustion with CO_2 capture for combined cooling, heating and power production. Appl. Energy 195. https://doi.org/10.1016/j.apenergy.2017.03.093.

Fan, L.S., 2010. Chemical looping systems for fossil energy conversions. Chem. Looping Syst. Foss. Energy Convers. https://doi.org/10.1002/9780470872888.

Franco, C., Pinto, F., Gulyurtlu, I., Cabrita, I., 2003. The study of reactions influencing the biomass steam gasification process. Fuel 82. https://doi.org/10.1016/S0016-2361(02)00313-7.

Ge, Y., He, T., Wang, Z., Han, D., Li, J., Wu, Jingli, Wu, Jinhu, 2020a. Chemical looping oxidation of CH4 with 99.5 % CO selectivity over V2O3-based redox materials using CO_2 for regeneration. AIChE J. 66. https://doi.org/10.1002/aic.16772.

Ge, Y., He, T., Wang, Z., Han, D., Li, J., Wu, Jingli, Wu, Jinhu, 2020b. Chemical looping oxidation of CH4 with 99.5 % CO selectivity over V2O3-based redox materials using CO_2 for regeneration. AIChE J. 66. https://doi.org/10.1002/aic.16772.

Ghosh Ray, S., Ghangrekar, M.M., 2019a. Comprehensive review on treatment of high-strength distillery wastewater in advanced physico-chemical and biological degradation pathways. Int. J. Environ. Sci. Technol. https://doi.org/10.1007/s13762-018-1786-8.

Ghosh Ray, S., Ghangrekar, M.M., 2019b. Comprehensive review on treatment of high-strength distillery wastewater in advanced physico-chemical and biological degradation pathways. Int. J. Environ. Sci. Technol. https://doi.org/10.1007/s13762-018-1786-8.

Guo, Q., Hu, X., Liu, Y., Jia, W., Yang, M., Wu, M., Tian, H., Ryu, H.J., 2015. Coal chemical-looping gasification of Ca-based oxygen carriers decorated by CaO. Powder Technol. 275. https://doi.org/10.1016/j.powtec.2015.01.061.

Hakandai, C., Sidik Pramono, H., Aziz, M., 2022. Conversion of municipal solid waste to hydrogen and its storage to methanol. Sustain. Energy Technol. Assess. 51. https://doi.org/10.1016/j.seta.2022.101968.

Huang, Z., He, F., Feng, Y., Zhao, K., Zheng, A., Chang, S., Wei, G., Zhao, Z., Li, H., 2014. Biomass char direct chemical looping gasification using NiO-modified iron ore as an oxygen carrier. Energy Fuels. https://doi.org/10.1021/ef401528k.

Huang, Z., Deng, Z., Chen, D., He, F., Liu, S., Zhao, K., Wei, G., Zheng, A., Zhao, Z., Li, H., 2017a. Thermodynamic analysis and kinetic investigations on biomass char chemical looping gasification using Fe-Ni bimetallic oxygen carrier. Energy 141. https://doi.org/10.1016/j.energy.2017.11.127.

Huang, Z., Xu, G., Deng, Z., Zhao, K., He, F., Chen, D., Wei, G., Zheng, A., Zhao, Z., Li, H., 2017b. Investigation on gasification performance of sewage sludge using chemical looping gasification with iron ore oxygen carrier. Int. J. Hydrog. Energy 42. https://doi.org/10.1016/j.ijhydene.2017.08.133.

Inayat, A., Ahmad, M.M., Yusup, S., Mutalib, M.I.A., 2010. Biomass steam gasification with in-situ CO_2 capture for enriched hydrogen gas production: a reaction kinetics modelling approach. Energies 3. https://doi.org/10.3390/en3081472.

Jiang, P., Berrouk, A.S., Dara, S., 2019. Biomass gasification integrated with chemical looping system for hydrogen and power. coproduction process – thermodynamic and techno-economic assessment. Chem. Eng. Technol. 42. https://doi.org/10.1002/ceat.201900130.

Kale, G.R., Kulkarni, B.D., Bharadwaj, K. v, 2013. Chemical looping reforming of ethanol for syngas generation: a theoretical investigation. Int. J. Energy Res. 37. https://doi.org/10.1002/er.1958.

Kaza, S., Yao, L.C., Bhada-Tata, P., van Woerden, F., 2018. What a Waste 2.0: A Global Snapshot of Solid Waste Management to 2050, What a Waste 2.0: A Global Snapshot of Solid Waste Management to 2050. https://doi.org/10.1596/978–1-4648–1329-0.

Krenzke, P.T., Fosheim, J.R., Davidson, J.H., 2017. Solar fuels via chemical-looping reforming. Sol. Energy 156. https://doi.org/10.1016/j.solener.2017.05.095.

Luo, S., Zeng, L., Xu, D., Kathe, M., Chung, E., Deshpande, N., Qin, L., Majumder, A., Hsieh, T.L., Tong, A., Sun, Z., Fan, L.S., 2014. Shale gas-to-syngas chemical looping process for stable shale gas conversion to high purity syngas with a H2:CO ratio of 2: 1. Energy Environ. Sci. 7. https://doi.org/10.1039/c4ee02892a.

Mattisson, T., Keller, M., Linderholm, C., Moldenhauer, P., Rydén, M., Leion, H., Lyngfelt, A., 2018. Chemical-looping technologies using circulating fluidized bed

systems: status of development. Fuel Process. Technol. https://doi.org/10.1016/j.fuproc.2017.11.016.
Mehrpooya, M., Moftakhari Sharifzadeh, M.M., Rajabi, M., Aghbashlo, M., Tabatabai, M., Hosseinpour, S., Ramakrishna, S., 2017. Design of an integrated process for simultaneous chemical looping hydrogen production and electricity generation with CO_2 capture. Int. J. Hydrog. Energy 42. https://doi.org/10.1016/j.ijhydene.2016.12.093.
Mohamed, U., Zhao, Y., Huang, Y., Cui, Y., Shi, L., Li, C., Pourkashanian, M., Wei, G., Yi, Q., Nimmo, W., 2020. Sustainability evaluation of biomass direct gasification using chemical looping technology for power generation with and w/o CO_2 capture. Energy 205. https://doi.org/10.1016/j.energy.2020.117904.
Mohamed, U., Zhao, Y. jie, Yi, Q., Shi, L. juan, Wei, G. qing, Nimmo, W., 2021. Evaluation of life cycle energy, economy and CO_2 emissions for biomass chemical looping gasification topower generation. Renew. Energy 176. https://doi.org/10.1016/j.renene.2021.05.067.
More, A., Veser, G., 2017. Physical mixtures as simple and efficient alternative to alloy carriers in chemical looping processes. AIChE J. 63. https://doi.org/10.1002/aic.15380.
Najera, M., Solunke, R., Gardner, T., Veser, G., 2011. Carbon capture and utilization via chemical looping dry reforming. Chem. Eng. Res. Des. 89. https://doi.org/10.1016/j.cherd.2010.12.017.
Otsuka, K., Wang, Y., Sunada, E., Yamanaka, I., 1998. Direct partial oxidation of methane to synthesis gas by cerium oxide. J. Catal. 175. https://doi.org/10.1006/jcat.1998.1985.
Phuong, T., le, Besson, M., 2019. Catalytic wet air oxidation using supported Pt and Ru catalysts for treatment of distillery wastewater (CoGnAc and sugarcane vinasses). Energies 12. https://doi.org/10.3390/en12203974.
Prasad, B.V.R.K., Kuester, J.L., 1988. Process analysis of a dual fluidized bed biomass gasification system. Ind. Eng. Chem. Res. 27. https://doi.org/10.1021/ie00074a016.
Qin, W., Wang, Y., Lin, C., Hu, X., Dong, C., 2015. Possibility of morphological control to improve the activity of oxygen carriers for chemical looping combustion. Energy Fuels 29. https://doi.org/10.1021/ef5024934.
Qin, W., Wang, J., Luo, L., Liu, L., Xiao, X., Zheng, Z., Sun, S., Hu, X., Dong, C., 2018. Chemical looping reforming of ethanol-containing organic wastewater for high ratio H<inf>2</inf>/CO syngas with iron-based oxygen carrier. Int. J. Hydrog. Energy 43. https://doi.org/10.1016/j.ijhydene.2018.05.080.
Qin, W., Wang, J., Gao, Q., Jiao, L., Chen, X., Chen, S., Jia, K., Xiao, X., Zheng, Z., Zhao, J., Liu, L., Dong, C., 2019b. Corn-stalk chemical looping combustion using tert-butanol waste solution. Energy Fuels 33. https://doi.org/10.1021/acs.energyfuels.8b03948.
Qin, W., Luo, L., Chen, S., Iqbal, T., Xiao, X., Dong, C., 2021. Efficient strategy of utilizing alkaline liquid waste boosting biomass chemical looping gasification to produce hydrogen. Fuel Process. Technol. 217. https://doi.org/10.1016/j.fuproc.2021.106818.
Qin, Wu, Chen, S., Ma, B., Wang, J., Li, J., Liang, R., Xu, Z., Liu, L., Dong, C., Zhang, H., 2019a. Methanol solution promoting cotton fiber chemical looping gasification for high H2/CO ratio syngas. Int. J. Hydrog. Energy 44. https://doi.org/10.1016/j.ijhydene.2019.01.267.
Ranjbari, M., Shams Esfandabadi, Z., Quatraro, F., Vatanparast, H., Lam, S.S., Aghbashlo, M., Tabatabaei, M., 2022. Biomass and organic waste potentials towards implementing circular bioeconomy platforms: a systematic bibliometric analysis. Fuel 318, 123585. https://doi.org/10.1016/J.FUEL.2022.123585.
Ratna, S., Rastogi, S., Kumar, R., 2021. Current trends for distillery wastewater management and its emerging applications for sustainable environment. J. Environ. Manag. https://doi.org/10.1016/j.jenvman.2021.112544.
Rodriguez-Caballero, A., Ramond, J.B., Welz, P.J., Cowan, D.A., Odlare, M., Burton, S.G., 2012. Treatment of high ethanol concentration wastewater by biological sand filters: Enhanced COD removal and bacterial community dynamics. J. Environ. Manag. 109, 54–60. https://doi.org/10.1016/J.JENVMAN.2012.05.005.
Samprón, I., de Diego, L.F., García-Labiano, F., Izquierdo, M.T., Abad, A., Adánez, J., 2020. Biomass chemical looping gasification of pine wood using a synthetic Fe2O3/Al2O3 oxygen carrier in a continuous unit. Bioresour. Technol. 316. https://doi.org/10.1016/j.biortech.2020.123908.
Samprón, I., de Diego, L.F., García-Labiano, F., Izquierdo, M.T., 2021. Optimization of synthesis gas production in the biomass chemical looping gasification process operating under auto-thermal conditions. Energy 226. https://doi.org/10.1016/j.energy.2021.120317.
Shen, L., Gao, Y., Xiao, J., 2008. Simulation of hydrogen production from biomass gasification in interconnected fluidized beds. Biomass Bioenergy 32. https://doi.org/10.1016/j.biombioe.2007.08.002.
Song, C., Hu, X., Liu, Z., Li, S., Kitamura, Y., 2020. Combination of brewery wastewater purification and CO_2 fixation with potential value-added ingredients production via different microalgae strains cultivation. J. Clean. Prod. 268. https://doi.org/10.1016/j.jclepro.2020.122332.
Udomsirichakorn, J., Salam, P.A., 2014. Review of hydrogen-enriched gas production from steam gasification of biomass: the prospect of CaO-based chemical looping gasification. Renew. Sustain. Energy Rev. https://doi.org/10.1016/j.rser.2013.10.013.
de Vos, Y., Jacobs, M., van der Voort, P., van Driessche, I., Snijkers, F., Verberckmoes, A., 2019. Sustainable iron-based oxygen carriers for chemical looping for hydrogen generation. Int. J. Hydrog. Energy 44. https://doi.org/10.1016/j.ijhydene.2018.11.099.
Yan, J., Sun, R., Shen, L., Bai, H., Jiang, S., Xiao, Y., Song, T., 2020. Hydrogen-rich syngas production with tar elimination via biomass chemical looping gasification (BCLG) using BaFe2O4/Al2O3 as oxygen carrier. Chem. Eng. J. 387. https://doi.org/10.1016/j.cej.2020.124107.
Yan, L., Cao, Y., Li, X., He, B., 2018. Characterization of a dual fluidized bed gasifier with blended biomass/coal as feedstock. Bioresour. Technol. 254. https://doi.org/10.1016/j.biortech.2018.01.067.
Zaini, I.N., Nurdiawati, A., Aziz, M., 2017. Cogeneration of power and H2 by steam gasification and syngas chemical looping of macroalgae. Appl. Energy 207. https://doi.org/10.1016/j.apenergy.2017.06.071.
Zeng, J., Xiao, R., Zeng, D., Zhao, Y., Zhang, H., Shen, D., 2016. High H2/CO ratio syngas production from chemical looping gasification of sawdust in a dual fluidized bed gasifier. Energy Fuels 30. https://doi.org/10.1021/acs.energyfuels.5b02204.
Zhang, R., Zhang, J., Guo, W., Wu, Z., Wang, Z., Yang, B., 2021. Effect of torrefaction pretreatment on biomass chemical looping gasification (BCLG) characteristics: gaseous products distribution and kinetic analysis. Energy Convers. Manag. 237. https://doi.org/10.1016/j.enconman.2021.114100.
Zhao, X., Zhou, H., Sikarwar, V.S., Zhao, M., Park, A.H.A., Fennell, P.S., Shen, L., Fan, L. S., 2017. Biomass-based chemical looping technologies: the good, the bad and the future. Energy Environ. Sci. https://doi.org/10.1039/c6ee03718f.
Zheng, Y., Li, K., Wang, H., Tian, D., Wang, Y., Zhu, X., Wei, Y., Zheng, M., Luo, Y., 2017. Designed oxygen carriers from macroporous LaFeO3 supported CeO2 for chemical-looping reforming of methane. Appl. Catal. B Environ. 202. https://doi.org/10.1016/j.apcatb.2016.08.024.
Zheng, Z., Luo, L., Chen, S., Qin, W., Dong, C., Xiao, X., 2020a. Activating Fe<inf>2</inf>O<inf>3</inf> using K<inf>2</inf>CO<inf>3</inf>-containing ethanol solution for corn stalk chemical looping gasification to produce hydrogen. Int. J. Hydrog. Energy 45. https://doi.org/10.1016/j.ijhydene.2020.05.226.
Zheng, Z., Luo, L., Feng, A., Iqbal, T., Li, Z., Qin, W., Dong, C., Zhang, S., Xiao, X., 2020b. CaO-assisted alkaline liquid waste drives corn stalk chemical looping gasification for hydrogen production. ACS Omega 5. https://doi.org/10.1021/acsomega.0c02787.